Charge density wave and charge pump of interacting fermions in circularly shaken hexagonal optical lattices

Tao Qin,[1] Alexander Schnell,[2] Klaus Sengstock,[3, 4, 5] Christof Weitenberg,[3, 4] André Eckardt,[2] and Walter Hofstetter[1]

[1]Institut für Theoretische Physik, Goethe-Universität, 60438 Frankfurt/Main, Germany
[2]Max-Planck-Institut für Physik komplexer Systeme, Nöthnitzer Straße 38, 01187 Dresden, Germany
[3]Institut für Laserphysik (ILP), Universität Hamburg,
Luruper Chaussee 149, 22761 Hamburg, Germany
[4]Hamburg Centre for Ultrafast Imaging, Luruper Chaussee 149, 22761 Hamburg, Germany
[5]Zentrum für Optische Quantentechnologien (ZOQ),
Universität Hamburg, Luruper Chaussee 149, 22761 Hamburg, Germany

We analyze strong correlation effects and topological properties of interacting fermions with a Falicov-Kimball type interaction in circularly shaken hexagonal optical lattices, which can be effectively described by the Haldane-Falicov-Kimball model, using the real-space Floquet dynamical mean-field theory (DMFT). The Haldane model, a paradigmatic model of the Chern insulator, is experimentally relevant, because it has been realized using circularly shaken hexagonal optical lattices. We show that in the presence of staggering a charge density wave emerges, which is affected by interactions and resonant tunneling. We demonstrate that interactions smear out the edge states by introducing a finite life time of quasiparticles. Even though a general method for calculating the topological invariant of a nonequilibrium steady state is lacking, we extract the topological invariant using a Laughlin charge pump set-up. We find and attribute to the dissipations into the bath connected to every lattice site, which is intrinsic to real-space Floquet DMFT methods, that the pumped charge is not an integer even for the non-interacting case at very low reservoir temperatures. Furthermore, using the rate equation based on the Floquet-Born-Markov approximation, we calculate the charge pump from the rate equations for the non-interacting case to identify the role of the spectral properties of the bath. Starting from this approach we propose an experimental protocol for measuring quantized charge pumping.

I. INTRODUCTION

Time periodically driven ultracold atoms in optical lattices are a versatile and powerful platform to simulate models with non-trivial topological properties [1, 2]. Two paradigmatic models, the Hofstadter model and the Haldane model have been realized with Raman laser assisted tunneling [3–5] and circularly shaken hexagonal lattices [6–8], respectively. Different techniques have been developed in setups with ultracold atoms in optical lattices to detect topological properties. Using a drift measurement, the topology of the lowest band of the Hofstadter model was determined [5]. By measuring the shift of atom clouds in a one-dimensional superlattice, the Thouless charge pump was realized in bosonic [9, 10] and fermionic [11] systems. A two-dimensional version of the topological charge pump was demonstrated by mapping a four-dimensional quantum Hall system to a two-dimensional square superlattice using dimensional reduction [12]. Using the tomographic technique that was first proposed in Ref. [13], the Berry curvature of the Haldane model was mapped out in momentum space [7]. Also, dynamical vortices due to quenching into the Floquet Hamiltonian were observed [8], which are a non-equilibrium signature of topology. The trajectories of the dynamical vortices in momentum space were used to determine the linking number [14], which can be directly related to the Chern number of the Hamiltonian after a quench [15].

Introducing two-particle interactions into a time-periodically driven system is a highly non-trivial problem from the point of view of both experiment and theory. In experiments one needs to overcome the problem of heating. It was shown that an interacting time-periodically driven closed system will heat up to a trivial state with infinite temperature [16, 17], with only a few exceptions like many-body localized systems [18, 19], integrable systems [20] and the prethermalization plateau [21, 22]. Multi-photon interband heating has been observed in a shaken 1D optical lattice [23]. Resonant tunneling, which happens when interactions are integer multiples of the driving frequency and magnetic correlations have been measured for strongly correlated fermions in hexagonal optical lattices with periodic driving in one direction [24]. Floquet evaporative cooling was shown to reduce heating for interacting bosons in a one-dimensional optical lattice [25]. However, there are no artificial gauge fields in these setups. Further efforts are needed to go into the interacting regime and realize an interacting system with artificial gauge fields. Theoretically, in the high-frequency limit, where the time periodically driven system is supposed to be in a prethermalized regime [21], the system can be described by an effective Hamiltonian in high-frequency approximation [26–28]. With interactions turned on, the interacting Haldane model can be studied with the static mean-field approximation [29, 30] and exact diagonalization [31]. The possible drawback of the effective Hamiltonian approach is that it cannot describe the non-equilibrium properties of the system. In the strongly correlated regime, one can obtain the effective

low-energy Hamiltonian in the limit of large interaction using a high-frequency expansion, which is equivalent to a Schrieffer-Wolff transformation [32]. With it one can qualitatively analyze the properties of near-resonant and resonant tunneling. However, to solve the low energy effective Hamiltonian is still a very non-trivial many-body problem. Numerical tools such as quantum Monte-Carlo and density matrix renormalization method need to be adopted to solve it.

Based on the experimental progress [7, 8, 14], we investigate non-equilibrium steady states (NESS) of fermions with Falicov-Kimball type interactions in a circularly shaken hexagonal optical lattice in a non-perturbative way using the method of real-space Floquet dynamical mean field theory (DMFT) [33–37], which can deal with driving, interactions and dissipation on equal footing. We study the strong correlation effects and topological properties of the system. We investigate the charge density wave (CDW) induced by the staggered potential as a function of increasing interactions. To study topological properties, we use a Laughlin charge pump setup [38], where a flux is inserted in the direction of the axis of a cylinder geometry. We observe how the edge states are smeared out by interactions. Furthermore, we calculate the charge pump due to insertion of flux quanta for different interactions. The dissipation into the bath makes the pumped charge non-integer. In addition, we study the role of dissipation for the non-interacting case in the presence of a heat bath using rate equations based on the Floquet-Born-Markov approximation. We start from an initial state which is close to equilibrium, and ramp up the flux adiabatically to calculate the pumped charge. By comparison with the equilibrium case we believe our procedure is experimentally practical.

We include a bath in all our calculations. While the bath prevents serious heating of the driven system, it causes dissipation which smears the integer charge pump, at least within our theoretical approaches for dealing with the bath. Whether it is possible to recover the integer charge pump by bath engineering will be a future direction.

The manuscript is organized as follows. In Sec. II, we present the model and methods used in our calculations. We outline the real-space Floquet DMFT method for the interacting and driven system, and the rate equation for the non-interacting case. In Sec. III, we present our results on the charge density wave and charge pump for the interacting system. For the non-interacting case, we show calculations from rate equations. We conclude in Sec. IV.

II. MODEL AND METHODS

A. The model

We start with a model for fermions in circularly shaken hexagonal optical lattices which can describe the experi-

mental setups described in Refs. [7, 8, 14, 39]

$$H_0 = -J \sum_{\langle ll' \rangle} c_{l'}^\dagger c_l + \sum_l \nu_l(t) n_l + \alpha(\Omega + \Delta) \sum_l \lambda_l n_l, \quad (1)$$

where l and l' label lattices sites, and $n_l = c_l^\dagger c_l$. Ω is the driving frequency and Δ is the detuning between the driving frequency and the AB-offset in the static lattice. $\lambda_{A(B)} = 0\,(1)$ for A and B sites in the unit-cell. $\alpha = \pm 1$ which is the sign of the staggered potential. We consider a near-resonant driving, which reestablishes resonant tunneling between A and B sites. The driving term is given by $\nu_l(t) = -\boldsymbol{r}_l \cdot \boldsymbol{F}(t) = -\boldsymbol{r}_l \cdot F[\cos(\Omega t)\,\hat{\boldsymbol{e}}_x + \tau \sin(\Omega t)\,\hat{\boldsymbol{e}}_y]$, where $\tau = \pm 1$ corresponds to counter-clockwise (clockwise) shaking. In the following, we choose $\alpha = 1$ and $\tau = 1$. We set the hopping amplitude $|J| = 1$ as the energy unit. For the Schrödinger equation of the system $i\frac{d|\psi\rangle}{dt} = H_0|\psi\rangle$, with the unitary transformation $|\psi\rangle = \mathcal{U}|\tilde{\psi}\rangle$ and $\mathcal{U} = e^{i\sum_l \tilde{\chi}_l(t)n_l}$, where

$$\tilde{\chi}_l(t) = -\int_0^t \tilde{\nu}_l(t)\,dt + \frac{1}{\mathcal{T}} \int_0^{\mathcal{T}} dt'' \int_0^{t''} dt' \tilde{\nu}_l(t'), \quad (2)$$

$$\tilde{\nu}_l(t) = \nu_l(t) + \alpha\Omega\lambda_l, \quad (3)$$

and $\mathcal{T} = \frac{2\pi}{\Omega}$, we have $\tilde{H}_0 = \mathcal{U}^\dagger H_0 \mathcal{U} - i\mathcal{U}^\dagger \frac{d}{dt}\mathcal{U}$. Therefore,

$$\tilde{H}_0 = -J \sum_{\langle ll' \rangle} e^{i\tilde{\theta}_{l'l}(t)} c_{l'}^\dagger c_l + \alpha\Delta \sum_l \lambda_l n_l \quad (4)$$

where $\tilde{\theta}_{l'l}(t) = \frac{K}{\Omega}\sin(\Omega t - \tau\phi_{l'l}) + \alpha\epsilon_{l'l}\Omega t - \alpha\epsilon_{l'l}\pi$. $\phi_{l'l}$ is defined by $\boldsymbol{r}_{l'} - \boldsymbol{r}_l = \cos(\phi_{l'l})\,\hat{\boldsymbol{e}}_x + \sin(\phi_{l'l})\,\hat{\boldsymbol{e}}_y$ for nearest neighbors. The corresponding effective Hamiltonian in second-order high-frequency approximation has been shown to be a Haldane-type Hamiltonian [14]. We then transform the Hamiltonian (4) to the Floquet space with $c_l = \sum_{n=-\infty}^{\infty} e^{-in\Omega t} c_{ln}$, so

$$\tilde{H}_0^{m_1 m_2} = -J \sum_{\langle ll' \rangle} \mathcal{J}_{m_2 - m_1 - \epsilon_{l'l}}\left(\frac{K}{\Omega}\right) e^{-i\Phi_{l'l}^{m_1 m_2}} c_{l'm_1}^\dagger c_{lm_2} \quad (5)$$

where $\Phi_{l'l}^{m_1 m_2} = (m_2 - m_1 - \epsilon_{l'l})\tau\phi_{l'l} + \pi\epsilon_{l'l}$. We set $\epsilon_{l'l} = \lambda_{l'} - \lambda_l$. $\mathcal{J}_{m_2 - m_1 - \epsilon_{l'l}}\left(\frac{K}{\Omega}\right)$ is the Bessel function of the order $m_2 - m_1 - \epsilon_{l'l}$. m_1 and m_2 are Floquet indices.

We consider a Falicov-Kimball interaction, where the mobile atoms interact with localized atoms:

$$H_{int} = U \sum_l c_l^\dagger c_l f_l^\dagger f_l. \quad (6)$$

U is the interaction strength. f_l $(f_l^\dagger)$ is the annihilation (creation) operator for localized atoms.

B. Real-space Floquet DMFT

We outline the real-space Floquet DMFT method that we adopt to deal with the Falicov-Kimball interaction [33,

34, 40, 41]. It is a method to study the NESS in an inhomogeneous system. To reach the NESS, every lattice site is coupled to a bath. We use a free-fermion bath in our implementation [37, 42]. The full Green's function of the lattice system satisfies Dyson's equation,

$$\left(\hat{G}^{-1}\right)_{ll',mn}(\omega) = \left(\hat{G}_0^{-1}\right)_{ll',mn}(\omega) - \hat{\Sigma}_{l,mn}(\omega)\,\delta_{ll'}$$
$$- \hat{\Sigma}_{\text{bath},l,mn}(\omega)\,\delta_{ll'} \qquad (7)$$

where every part is defined on the Keldysh contour [43] and in Floquet space

$$\hat{G}(\omega) = \begin{pmatrix} G^R & G^K \\ 0 & G^A \end{pmatrix}(\omega). \qquad (8)$$

$\omega \in \left[-\frac{\Omega}{2}, \frac{\Omega}{2}\right)$ is in the first Brillouin zone of Ω. For the non-interacting part we have

$$G_{0ll',mn}^{R-1}(\omega) = \left(\omega + n\Omega + i0^+\right)\delta_{mn}\delta_{ll'} - \tilde{H}_{0ll',mn}, \quad (9)$$

and $G_0^A(\omega) = G_0^{R\dagger}(\omega)$, as well as $\left(G_0^{-1}(\omega)\right)^K = 0$ [37, 42]. $\Sigma_{\text{bath},l,mn}(\omega)$ is the correction to the self-energy on site l due to dissipation to the bath

$$\Sigma_{\text{bath},l,mn}(\omega) = \begin{pmatrix} i\Gamma\delta_{mn} & -2i\Gamma F_n(\omega)\,\delta_{mn} \\ 0 & -i\Gamma\delta_{mn} \end{pmatrix}, \quad (10)$$

assuming that the density of states (DOS) of the bath is constant. Γ is a phenomenological dissipation rate to the bath, and $F_n(\omega) = \tanh\frac{\omega + n\Omega}{k_B T}$ where T is the temperature of the bath [37]. $\Sigma_{l,mn}(\omega)$ is the lattice self-energy due to two-particle interactions and is obtained from the impurity solver for every lattice site l:

$$G_l(\omega) = w_0 \mathcal{G}_{0,l}(\omega) + w_1 \left[\mathcal{G}_{0,l}^{-1}(\omega) - U\right]^{-1} \qquad (11)$$

where w_1 is the probability of one site being occupied by immobile atoms and $w_0 = 1 - w_1$. In the following, we focus on the case of half filling, for which $w_1 = \frac{1}{2}$ and $w_0 = \frac{1}{2}$. The self-consistent loop is closed by

$$\mathcal{G}_{0,l}^{-1}(\omega) = G_l^{-1}(\omega) + \Sigma_l(\omega). \qquad (12)$$

C. Rate Equations in presence of heat bath

Here we present a method of studying the NESS using rate equations for the non-interacting gas. Using this approach we will investigate the impact of the spectral properties of the bath on the non-equilibrium steady state of the system and the quantization of charge pumping.

In order to access situations where the particle number N of fermions in the system is conserved and there is only heat exchange with a thermal environment, we here present an alternative treatment using rate equations. This method only applies to the noninteracting Fermi gas, where $U = 0$.

Here, the total Hamiltonian reads

$$H(t) = \tilde{H}_0(t) + \sqrt{\Gamma} v \sum_\alpha \kappa_\alpha(b_\alpha^\dagger + b_\alpha) + \sum_\alpha \omega_\alpha b_\alpha^\dagger b_\alpha, \quad (13)$$

where the bath is modeled by a collection of harmonic oscillators b_α, corresponding frequencies ω_α and dimensionless coupling constants κ_α, and some system coupling operator v. Note that we have separated the strength $\sqrt{\Gamma}$ of the system–bath coupling from the coefficients κ_α. It turns out that the magnitude of the dissipation rate is given essentially by Γ.

In the weak system–bath coupling limit, $\Gamma \to 0$, we may perform the usual Born-Markov [44] and the full rotating wave approximation [45–47] in which we average over the long relaxation time scales $\propto 1/\Gamma$ (rather than just one period of the driving). For a single fermion, $N = 1$, one then finds that the reduced system density matrix is asymptotically diagonal in the Floquet states $|a(t)\rangle$, i.e. $\varrho(t) = \sum_a p_a(t)|a(t)\rangle\langle a(t)|$, and the asymptotic dynamics is governed by a Pauli rate equation,

$$\partial_t p_a(t) = \sum_b \left[R_{ab}p_b(t) - R_{ba}p_a(t)\right], \qquad (14)$$

that describes the transfer between populations $p_a(t)$ of the Floquet states. This happens at a rate

$$R_{ab} = 2\pi\Gamma \sum_{m \in \mathbb{N}} |v_{ab}^{(m)}|^2 g(\varepsilon_a - \varepsilon_b - m\Omega), \qquad (15)$$

involving the quasienergy ε_a of Floquet state a and the m-th component of the Fourier transform of the coupling,

$$v_{ab}^{(m)} = \frac{1}{\mathcal{T}} \int_0^{\mathcal{T}} dt \langle a(t)|v|b(t)\rangle e^{im\Omega t}. \qquad (16)$$

It also enters the bath-correlation function g that reads for the phonon bath

$$g(E) = \begin{cases} J(E)n_B(E), & E > 0, \\ J(-E)(1 + n_B(-E)), & E < 0, \end{cases} \qquad (17)$$

with the occupation function $n_B(E) = 1/(e^{E/T} - 1)$ and the spectral density of the bath $J(E) = \sum_\alpha \kappa_\alpha^2 \delta(E - \omega_\alpha)$, for $E \geq 0$. Typical baths with a continuum of modes α obey

$$J(E) \propto E^d e^{-E/E_c}, \qquad (18)$$

where the exponent d controls the low-frequency behaviour of $J(E)$. Here $d = 1$ denotes the ohmic case and $d < 1$ ($d > 1$) is sub-(super-)ohmic. The high-frequency cutoff parameter E_c basically is set by the correlation time $\tau_B \propto 1/E_c$ of the bath [44]. In order to be consistent with the Markov approximation, this time τ_B must be small when compared to the typical time scale of relaxation $\tau_R \propto 1/\Gamma$, which is always valid in the weak coupling limit $\Gamma \to 0$ that we aim at.

The non-interacting Fermi gas may be considered in the same framework, however, one has to additionally

implement quantum statistics. This leads to the many particle version of the Pauli rate equation [48],

$$\partial_t \langle n_a \rangle = \sum_b R_{ab}(1-\langle n_a \rangle)\langle n_b \rangle - R_{ba}(1-\langle n_b \rangle)\langle n_a \rangle, \quad (19)$$

where $\langle n_a \rangle$ is the mean occupation of the Floquet state a and where we have applied the mean field approximation $\langle n_a n_b \rangle \approx \langle n_a \rangle \langle n_b \rangle$ discussed in Ref. [49]. The nonequilibrium steady state is found by solving for steady occupations, $\partial_t \langle n_a \rangle = 0$.

III. RESULTS AND DISCUSSIONS

A. Charge density wave

In this section, we focus on the effects of interactions and resonant tunneling on the charge density wave (CDW) induced by the staggered potential. We consider a two-dimensional hexagonal optical lattice with 9×9 unit cells and periodic boundary conditions in both x and y directions. The charge densities are different on A and B sites, with the definition of the charge density on site A (B) $N_i^c = \frac{1}{2\pi} \int_{-\Omega/2}^{\Omega/2} d\omega \sum_n G_{nn,i}^<(\omega)$, where $i = $ A (B), n is the Floquet index for the Floquet Green's function $G_{A(B)}^<(\omega)$ on site A (B), and $G_{nn,i}^<(\omega) = \frac{1}{2}(G_{nn,i}^K(\omega) - G_{nn,i}^R(\omega) + G_{nn,i}^A(\omega))$. Because of the periodic boundary conditions, there are only two different sites in the hexagonal optical lattice. Our study is different from those in Ref. [50–52], where the CDW order parameter is defined as $\Delta_{\mathrm{CDW}}^f = N_A^f - N_B^f$ because a finite density difference of localized f-atoms is needed to spontaneously break the symmetry between sublattice sites A and B. However, in our case of the real space implementation of DMFT calculations, we choose $w_1 = \frac{1}{2}$ for all sites. We nevertheless have a CDW also for $\Delta = 0$. Namely, for an integer α, i.e. in the presence of the staggered potential $\alpha \Omega \sum_l \lambda_l n_l$, will cause an effective energy offset between A and B sites (appearing in the second-order high-frequency expansion of the effective Hamiltonian [14]). It results from virtual second-order processes where a particle tunnels from an A (B) site to a neighboring B (A) site and back. In Fig. 1, we show a comparison calculation to prove this. We can see a perfect symmetry of the spectral functions for both A and B sites for the case without staggered potential, in contrast to a broken symmetry for the case when the staggered potential is present.

There is a rich relation between charge density and interactions. We show the charge density $N_{A(B)}$ with increasing interactions in Fig. 2. (i) When $U = 0$, the detuning Δ is the factor that affects occupation of A and B sites, and one can tune the occupations by changing Δ. (ii) We next discuss the case where $0 < U \lesssim 3$. The repulsive interaction U counteracts the effect of Δ, and the density difference is reduced. In this region, the resonant tunneling is suppressed because the bandwidth is
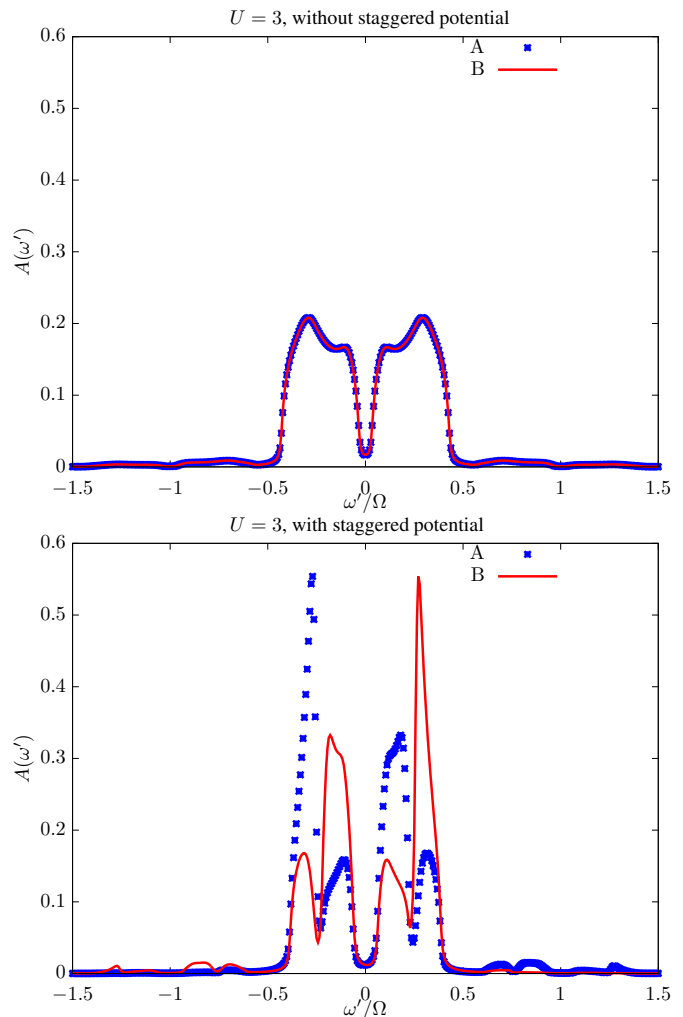

Figure 1: Spectral functions $A(\omega') = -\frac{1}{\pi}\mathrm{Im}G_{nn}^R(\omega)$ with $\omega' = \omega + n\Omega$ for the case without staggered potential (upper), and the case with staggered potential $\Omega \sum_l \lambda_l n_l$ (lower). For both panels, the driving frequency $\Omega = 7$, $\frac{K}{\Omega} = 1.28$, and $\Delta = 0$. Bath parameters are $\Gamma = T = 0.05$.

smaller than the driving frequency. We show the spectral functions for $U = 3$ in the lower panel of Fig. 1, and we observe that the band width is approximately Ω. The bandwidth is smaller than Ω for a smaller U. (iii) When $U \gtrsim 3$, resonant tunneling plays an important role. We define $N_{B(A)}^+ = \frac{1}{2\pi} \int_{-\Omega/2}^{\Omega/2} d\omega \sum_{n,\omega+n\Omega>0} \mathrm{Im}G_{nn,B(A)}^<(\omega)$, which corresponds to the faction of atoms occupying the upper Mott band. The reason for these excitations is the resonant tunneling induced by the hopping $\langle F| e^{i\tilde{\theta}_{BA}(t)} c_B^\dagger c_A |I\rangle$ between A and B sites in the correlated regime. If there were no such resonant tunneling, the fraction of atoms on A site would be estimated as $N_A - N_A^+ + N_B^+$, and similarly for B site it would be $N_B + N_A^+ - N_B^+$. If the estimation were accurate, we would have $N_A - N_A^+ + N_B^+ \approx N_B + N_A^+ - N_B^+ \approx 0.5$ for interactions $U \gtrsim 3$. As shown by blue and red dots in Fig. 2, we note that both $N_A - N_A^+ + N_B^+$ and $N_B + N_A^+ - N_B^+$ are close
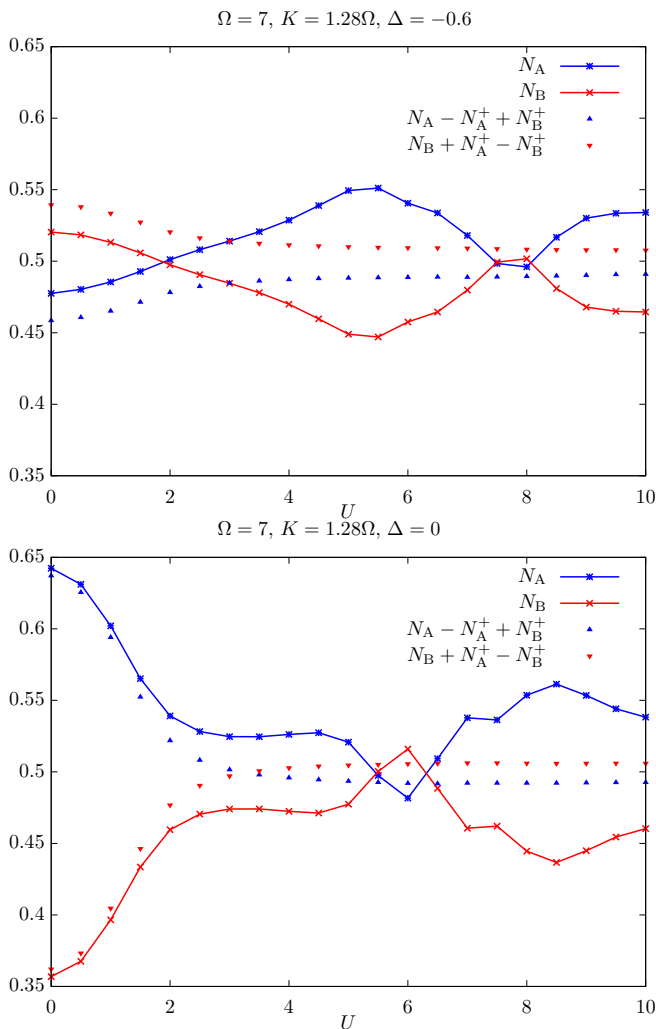
Figure 2: Charge density wave (CDW) versus interactions U for a two-dimensional hexagonal optical lattice with 9×9 unit cells and periodic boundary conditions in both x and y directions. Bath parameters are $\Gamma = T = 0.05$. $N_{A(B)}^+$ is shown in Fig. 3.

Figure 3: Charge density with positive frequency induced by resonant tunneling, plotted versus interactions U. The peak is due to one-photon resonant tunneling when $U = \Omega$. Other parameters are the same as in Fig. 2.

to 0.5 when $U \gtrsim 3$. This demonstrates that the resonant tunneling between A and B sites is the main contribution to the difference between the atom densities on A and B sites when U is relatively large. This shows the characteristic difference between the NESS and an equilibrium state. On the other hand, it offers a way to estimate the resonant tunneling. Suppose it is possible to measure the charge density N_A and N_B for different interactions. One can then estimate the contribution of the resonant tunneling by calculating $N_A - 0.5$ or $0.5 - N_B$ for $U \gtrsim 3$. (iii) There is some deviation from 0.5 for $N_A - N_A^+ + N_B^+$ and $N_B + N_A^+ - N_B^+$. It shows that there are high-order contributions, from the hopping A-B-A (or equivalently, B-A-B), to N_A^+ and N_B^+. These contributions do not affect the number of atoms on A and B sites, but create excitations. This is also evidence for that the next-nearest neighbor hopping is effectively generated by lattice shak-
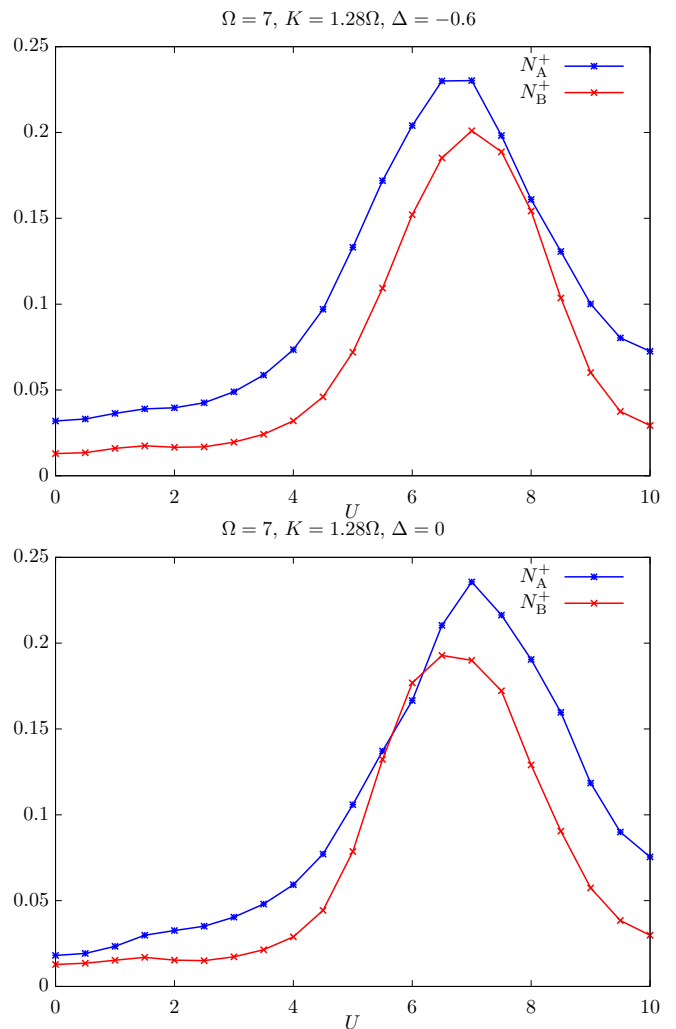
ing, even though in this calculation we cannot show that it comes with a phase in this calculation.

We have a short comment regarding the case in the upper panel of Fig. 1. When the staggered potential is absent, there are still resonant tunnelings. However, they are the same for A and B sites, in contrast to the case with staggered potentials.

In Fig. 3, the charge density with positive frequency ($N_{A(B)}^+ = \frac{1}{2\pi} \int_{-\Omega/2}^{\Omega/2} d\omega \sum_{n, \omega + n\Omega > 0} \mathrm{Im} G_{nn, A(B)}^< (\omega)$) is shown. It is corresponding to the effect of resonant tunneling [53]. The peak is at $U = \Omega = 7$, where the one-photon resonant tunneling is dominant. As we have discussed above, the contribution N_A^+ ($N_B^\dagger$) is due to the direct hopping from B (A) sites, plus higher-order contributions from A (B) sites. Generally, $N_A^+ > N_B^+$, and atoms prefer to hop to A sites due to the higher staggered potential on B sites.

B. Edge states

In this section, we present topological properties of a circularly shaken hexagonal optical lattice. We investigate edge states in a cylinder geometry of a hexagonal optical lattice, with a flux Φ insertion (Fig. 4) [54–56]. This is the setup in the Laughlin gedanken experiment [38]. The insertion of flux is equivalent to a twisted boundary condition in the direction with periodic boundary condition [57, 58]. It is a general setup with the potential to be generalized to disordered cases [58].

With insertion of one flux quantum, we demonstrate the change of topological properties of the system. Edge states are hallmarks of nontrivial topological properties. Using real-space Floquet DMFT, we study the interplay between interactions and edge states. We show the spectral functions in Fig. 5. For finite detuning Δ, the cylinder geometry can host edge states when $U = 0$. With increasing interactions, the edge states as a function of the inserted flux Φ are smeared out as can be seen in Fig. 5. This corresponds to a finite lifetime of quasiparticles. The sharp spectral peak of a quasiparticle is gradually expanded due to increasing interactions. When $U = 3$, we see a simple Mott gap. We observe three different phases: Chern insulator with edge states present, pseudogap metallic phase with gap closed, and Mott insulator with gap open again. According to the effective Hamiltonian [14], the ratio between the next-nearest neighbor hopping t_2 and nearest neighbor hopping t_1 is $|t_2/t_1| = 0.1$ with $|t_1| = 0.5$. The pseudogap metallic phase exists approximately when $U \approx 2$. This is consistent with DMFT calculations in Ref. [52] for the Haldane-Falicov-Kimball model. The difference is that here we are considering a non-equilibrium driven system connected to a bath. The largest interaction $U = 3$ we have shown is much smaller than driving frequency $\Omega = 7$. It can therefore be expected that resonant tunneling is greatly suppressed. The dissipation rate Γ into the bath has effects on the spectral functions especially for small U. It introduces an $i\Gamma$ correction to the self-energy and this term is equivalent to an interaction effect.
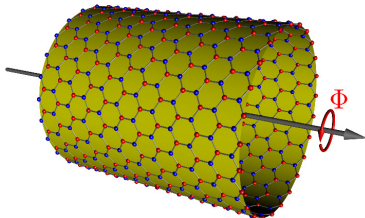

Figure 4: A cylinder geometry of a circularly shaken hexagonal optical lattice with a flux Φ insertion. This is the setup in the Laughlin gedanken experiment [38]. The zigzag boundary condition is used in the calculation.
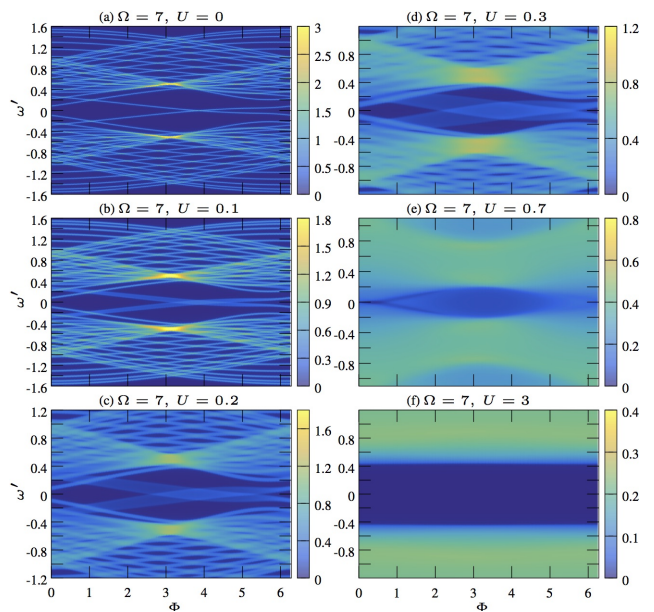

Figure 5: Spectral functions versus the flux Φ for different interactions. It shows interaction effects on edge states in a cylinder geometry of 3×10 unit cells with 3 unit cells in the direction with a periodical boundary condition. Other parameters are $\Omega = 7$, $\frac{K}{\Omega} = 1.28$, and $\Delta = -0.35$. Bath parameters are $\Gamma = 0.005$ and $T = 0.01$. ω' indicates a general frequency which can be outside the first Brillouin zone of Ω.

C. Charge pump

A second topological quantity which can be investigated in Laughlin's setup is the charge pump, which is closely related to edge states. For an equilibrium system, when well-defined edge states are present in the cylinder geometry of a hexagonal optical lattice, a change of one flux quantum will induce an integer number of atoms to transfer from one edge of the cylinder to the other [38]. The number of transferred atoms depends on the number of edge states. An integer charge pump is a signature of non-trivial topological phase. Following Ref. [54], we define the charge pump with insertion of flux Φ as

$$Q_\Phi = Q_{\mathcal{R},\Phi} - Q_{\mathcal{L},\Phi} \tag{20}$$

which is the charge density difference between two halves of the cylinder (see Fig. 6: left and right of the cylinder). $Q_{\alpha,\Phi} = \frac{1}{2\pi} \int_{-\Omega/2}^{\Omega/2} d\omega \sum_{i \in \alpha, n} \mathrm{Im} G_{i,\Phi,nn}^{<}(\omega)$ with $\alpha = \mathcal{R}, \mathcal{L}$, and Floquet index n. $\mathrm{Im} G_{i,\Phi,nn}^{<}(\omega) = \frac{1}{2}\mathrm{Im}\left[G_{i,\Phi,nn}^{K}(\omega) - G_{i,\Phi,nn}^{R}(\omega) + G_{i,\Phi,nn}^{A}(\omega)\right]$, where i is the site index in the left or right half. The flux is implemented according to Ref. [56]. Using the sum rule $\frac{1}{\pi} \int_{-\Omega/2}^{\Omega/2} d\omega \mathrm{Im} \sum_n G_{i,\Phi,nn}^{R/A} = 1$, we have

$$Q_\Phi = \int_{-\Omega/2}^{\Omega/2} d\omega \sum_n \frac{1}{2\pi} \mathrm{Im}\left[G_{\mathcal{R},\Phi,nn}^{K}(\omega) - G_{\mathcal{L},\Phi,nn}^{K}(\omega)\right]. \tag{21}$$
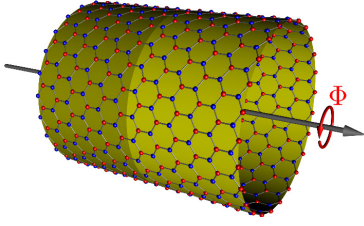
Figure 6: The charge pump with insertion of a flux Φ is defined as charge density difference $Q_\Phi = Q_{\mathcal{R},\Phi} - Q_{\mathcal{L},\Phi}$ between the two halves of the cylinder, as indicated by different background colors. When there are well-defined edge states, they are expected to be present in the left or the right half.

1. An isolated equilibrium system

We show that Q can indeed be a topological invariant to distinguish non-trivial and trivial topological phases for *an non-interacting equilibrium state*. For this case, no bath is needed for energy dissipation. We can determine the Keldysh Green's function using the fluctuation-dissipation theorem [43]: $G^K(\omega) = \tanh\frac{\beta_0\omega}{2}\left(G^R(\omega) - G^A(\omega)\right)$, where $\beta_0 = \frac{1}{k_B T_0}$ with T_0 the equilibrium temperature of the system. We choose T_0 as a very small number close to 0. The charge pump can be calculated as:

$$Q_\Phi = -\frac{1}{\pi}\mathrm{Im}\int_{-\Omega/2}^{\Omega/2} d\omega \sum_n f(\omega + n\Omega)$$
$$\times \mathrm{Im}\left[G^R_{\mathcal{R},\Phi,nn}(\omega) - G^R_{\mathcal{L},\Phi,nn}(\omega)\right]. \quad (22)$$

Q_Φ can be calculated directly or using the technique of the contour integral. In Fig. 7, we show the charge pump versus flux insertion Φ for topologically non-trivial and trivial cases. In the upper panel of Fig. 7, we observe a sharp jump of the charge density difference Q at the point Φ, where two edge states intersect each other. It means that one atom is transferred from one edge of the cylinder to the other. In contrast, in the topologically trivial case, we only observe a smooth change in the charge density. Therefore, Q_Φ can serve as a topological invariant for distinguishing topologically non-trivial and trivial cases.

2. System coupled to a free fermion bath

We present the charge pump Q for a NESS obtained from the real-space Floquet DMFT in Fig. 8. Corresponding to edge states in Fig. 5, we show that there is a jump in the charge pump in Fig. 8. However, the jump is not an integer even for very small interactions. With increasing interactions, the jump becomes very smooth. We explain why the jump is not integer even for $U = 0$. It does not contradict to what we show in Fig. 7. In real-space Floquet DMFT, there is a bath coupled to every lattice site. With the approximation of constant DOS of the bath, the dissipation into the bath introduces a finite
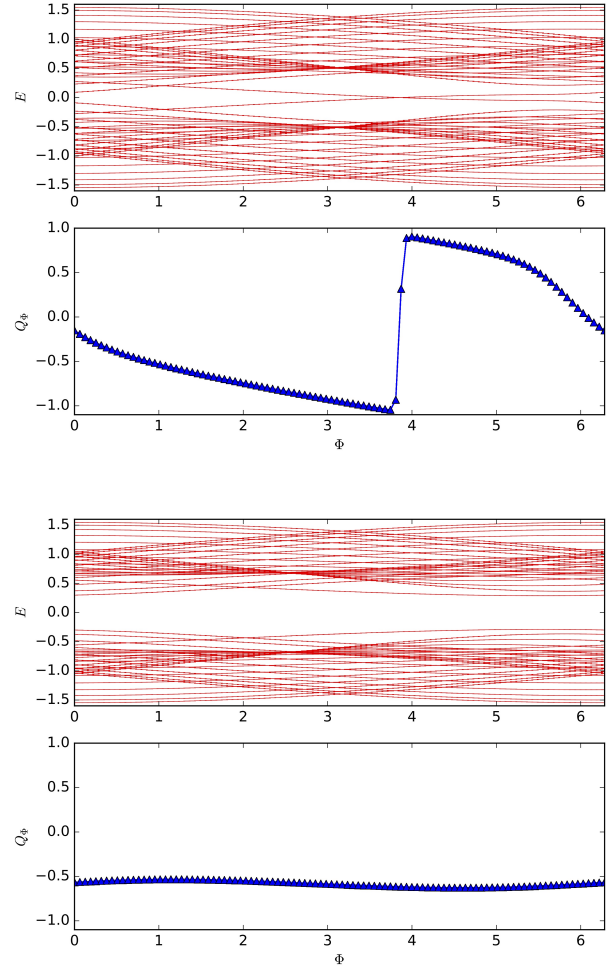

Figure 7: Charge pump Q_Φ with insertion of a flux for a cylinder hexagonal lattice with 3×10 unit cells in *an non-interacting equilibrium state*. There are 3 unit cells in the direction with periodic boundary conditions. Other parameters are $\Omega = 7$, $\frac{K}{\Omega} = 1.28$, $\Delta = -0.35$ (upper panel), and $\Delta = 0.35$ (lower panel).

self-energy to the system. This is equivalent to an interaction effect. In fact, it is this effective interaction which destroys the integer charge pump when $U = 0$. When the system couples to the environment (the bath) and becomes open, the unavoidable dissipation plays a role in the topological properties. Even though the dissipation is rather small, the interaction effect induced by it can be pronounced because the effective hopping is heavily dressed by the driving.

3. System coupled to a heat bath

To further identify the role of dissipation to the bath in the charge pump for a non-interacting system, we here study the NESS that forms when the driven system at
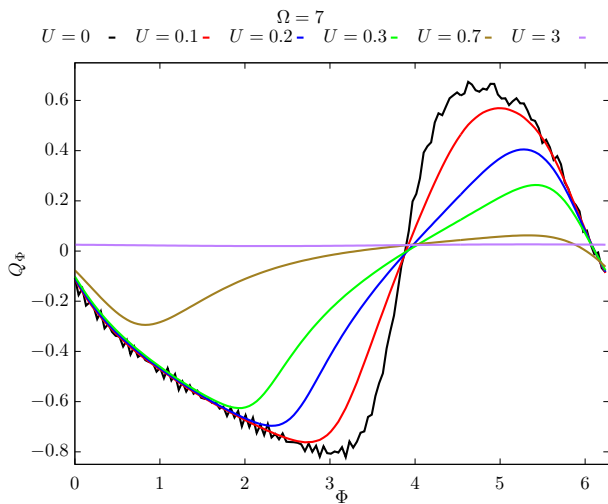
Figure 8: Charge pump Q_Φ with insertion of a flux Φ for a cylinder hexagonal lattice, obtained by real-space Floquet DMFT for different interactions. The parameters are the same as those in Fig. 5. For the non-interacting case, we obtain the charge pump by a direct calculation of the non-interacting Floquet Green's function with the bath corrections. It is different from the method of rate equations.

half filling is coupled to an ohmic heat bath, using the rate equations.

Similar to the fermionic reservoir, we couple one heat bath at temperature T to every site of the lattice. This is mediated by a coupling operator $v_{(l)} = c_l^\dagger c_l$ for a given site l. Note that we assume this form of the coupling for the direct frame. However, if we transform the coupling to the co-moving frame, it still obeys the same form since the unitary rotation $\mathcal{U}$ commutes with the coupling $c_l^\dagger c_l$. From Eq. (15) one then infers rates $R_{ab}^{(l)}$ that result from coupling this site l to the heat bath. The total rates for coupling the system globally to an external heat bath result from the incoherent sum of all of these processes, implying $R_{ab} = \sum_l R_{ab}^{(l)}$.

With these rates we solve the kinetic equation (19) for the NESS. Just to remind the reader, the resulting state is the long-time steady state that results when the system is under a constant driving and weakly coupled to the bath, meaning that the coupling constant is small when compared to all quasi-energy splittings in the system, $\sqrt{\Gamma} \ll (\varepsilon_k - \varepsilon_q)$, for $k \neq q$.

We observe that for frequencies Ω which are large when compared to the bandwidth, the distributions $\langle n_a \rangle$ that we observe in the NESS are still close to thermal distributions with an effective temperature T_{eff}, cf. the examples in Fig. 9(a) and (b). This effective temperature is obtained by fitting the closest thermal distribution to the occupations such that $\langle n_a \rangle \approx 1/(e^{(\varepsilon_a - \mu)/T_{\text{eff}}} + 1)$, and therefore assuming what was called a "Floquet-Gibbs" state in the literature [59]. Note that in Fig. 9, the temperature of the bath is $T = 0.001J$, but still, due to the driving, in the long-time limit the system heats
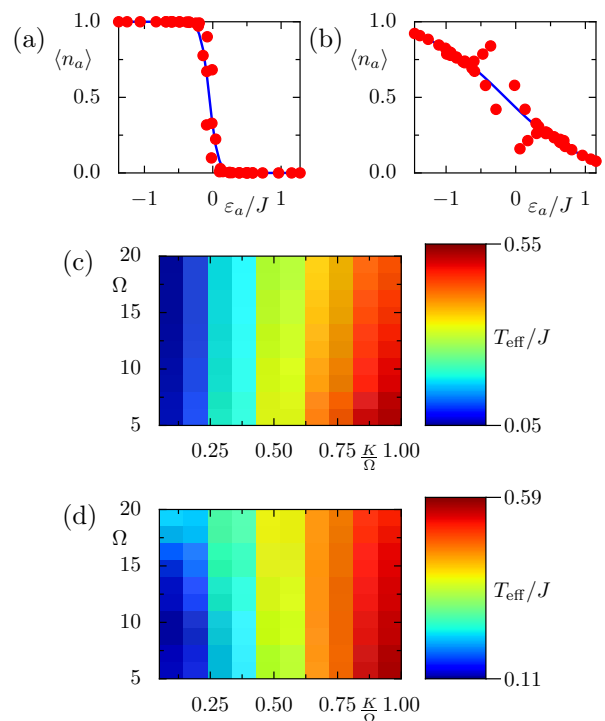

Figure 9: NESS that forms when the system is coupled to an ohmic heat bath (no cutoff, $E_c = \infty$) at $T = 0.001J$. (a, b) We obtain effective temperatures by fitting the distribution $\langle n_a \rangle$ (red dots) of the NESS with a Fermi-Dirac distribution with temperature T_{eff} (blue line), where (a) $\Delta = -0.1$, $\Omega = 5$, $K/\Omega = 0.05$ and (b) $\Delta = -0.3$, $\Omega = 13.33$, $K/\Omega = 1$. (c, d) T_{eff} as a function of driving parameters, for (c) $\Delta = -0.1J$ and (d) $\Delta = -0.3J$. We show states for a 3×7 lattice, but we observe that T_{eff} is almost independent of the size of the lattice.

up to quite high temperatures that are on the order of $T_{\text{eff}} \approx 0.1J$ as shown in Fig. 9(c) and (d) for a heat bath with ohmic spectral density and no spectral cutoff, $J(E) \propto E$. Interestingly, in this frequency regime, the effective temperature of the steady state seems to depend only on the relative strength K/Ω of the driving. Note that this is in contrast to the analytic formula that was presented in Ref. [60], where in addition to the K/Ω dependence they find a term that scales as $1/\Omega^d$ (where d is the exponent of the spectral density). In our calculations we also observe that T_{eff} is practically independent of the size of the lattice.

Even by further decreasing the temperature T of the bath, we are not able to reach lower effective temperatures T_{eff}. We checked this by comparing to the NESS for a hypothetic $T = 0$ bath, where there are no bath occupations $n_B = 0$, so that there is only spontaneous emission. These relatively large effective temperatures are detrimental for the observation of quantized charge pumping, since they correspond to a significant occupation of the "upper" Floquet band.

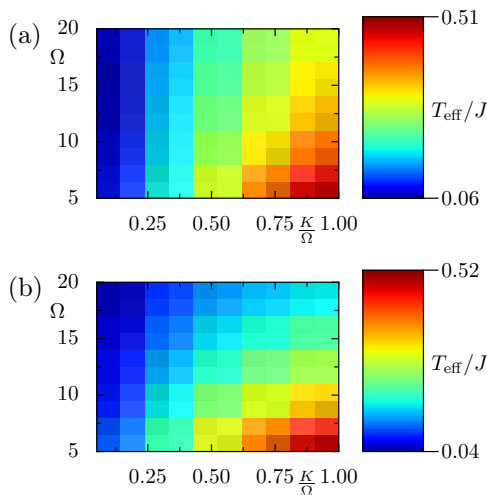Note that this heating is due to the population transfer between Floquet states that is induced due to the pres-

Figure 10: Like in Figure 9(d), but (a) with $J(E) \propto E^{0.5}$ and (b) with $J(E) \propto E \exp(-E/5J)$.

Figure 11: (a) Charge Pump Q_Φ with insertion of a flux Φ for parameters $\Omega = 20, \Delta = -0.1, K/\Omega = 0.25$ in a 3×10 lattice where we expect the system to be topological. For given flux Φ we let the system relax to the NESS in presence of a heat bath with $J(E) \propto E \exp(-E/E_c)$ and $T = 0.001J$. Using this procedure the signal is very weak, even though the effective temperature in the NESS are quite low. (b) However, there is a large transport signal if we prepare the NESS at $\Phi = 0$ and then ramp (at constant speed) one flux quantum within a finite ramp time $\tau \approx 50/J$. Here, the solid lines show snapshots of the system at integer multiples of $\mathcal{T}$ neglecting the micromotion. The green line (with some cutoff in the spectral density) features a relatively large charge transport that is close to the (almost) integer transport behavior that we expect for hypothetic thermal $T = 0$ populations of the quasienergies (dashed line).

ence of the coupling to the higher Floquet sidebands. As was pointed out in the literature [60–62], this heating can be suppressed by engineering the bath such that the spectral density $J(E)$ at large quasi-energy differences becomes smaller. For example if we suppose the bath is sub-ohmic with $J(E) \propto E^{0.5}$, as shown in Fig. 10(a), then at large frequencies Ω we find that heating is suppressed, leading to lower effective temperatures T_{eff} in the NESS. Similar suppression of heating is found in Fig. 10(b) for an ohmic bath, but with a finite cutoff $E_c = 5J$ in the spectral density $J(E) \propto E \exp(-E/E_c)$. Note that it has been argued in the literature that in the limit $\Omega \gg E_c$ resonances are suppressed and one an expects an effectively thermalized "Floquet-Gibbs" state [59]. Such a finite frequency cutoff is the manifestation of bath correlation times $\tau_R \propto 1/E_c$ that are on the order of the time scales of the system dynamics $\tau_S \propto 1/J$. Note that such finite correlation times are tunable e.g. in the case where the bath is a weakly interacting Bose-Einstein condensate in a trap. There, excitations are nicely described by Bogoliubuv quasiparticles (phonons) and the bath correlation times can be controlled by the trap frequency [63, 64]. Also, sympathetic cooling of fermions in Bose-Einstein condensates is a well established experimental technique, however there, typically a relatively strong coupling Γ is favorable, while here we target weak couplings.

If we now use a NESS that was prepared in presence of such a heat bath, one again may ask whether one can observe the underlying topological nature of the model. Similar to the DMFT calculations in presence of the fermionic reservoir, in Fig. 11(a) we show the charge difference Q_Φ of the right and lefthand side of the system in the NESS that was prepared for a given value of the flux Φ. However, even though for these parameters the model is topological and the effective temperatures are relatively low, especially in the case with a finite cutoff in the spectral density (green line), we do not see a
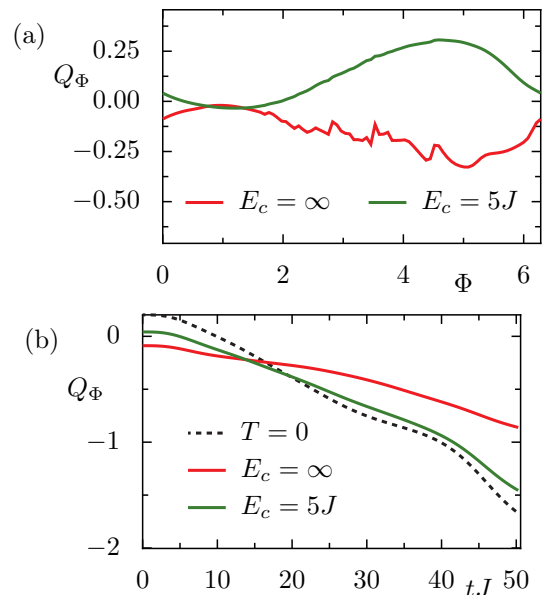
pronounced peak in the charge difference.

In order to overcome this problem, we propose a different strategy to probe topology in the model. Namely, in Fig. 11(a) it is assumed that the ramp time τ is big when compared to the relaxation times τ_R, i.e. we follow the system adiabatically in the thermodynamic sense. Here, since we are in the weak coupling regime where τ_R is large, we propose to perform a ramp on a much shorter time scale $\tau \ll \tau_R$, such that during the ramp one may neglect the action of the bath. However, this ramp should still be slow when compared to system time scales $\tau_s \ll \tau$, which one might call adiabatic in the closed system (without the presence of the bath). The solid lines in Fig. 11(b) show the charge transport that one observes in such a procedure, where we start with a NESS that is prepared without the presence of an external field, $\Phi_{\text{NESS}} = 0$. There, the values are quite high, for the ohmic bath with a cutoff. The density difference between two halve of the cylinder Q_Φ is up to about 1.4 (green line), corresponding to 0.7 of a charge is transported, which is very close to the quantized value that we expect for such a ramp

if we assume a $T = 0$ population of the quasi-energies (dashed line).

D. Experimental relevance

We discuss the possibilities to observe the physical quantities we have explored in an experiment. To detect the CDW, one can measure the local densities on A and B sites either in situ in a quantum gas microscope, after time of flight via adiabatic band mapping techniques, or via the double occupancy [65]. For the charge pump, one needs to compare the local particle density between two parts of the cylinder geometry. The extra flux, in fact, relaxes the requirement to have a periodic boundary condition in one direction. For a hexagonal lattice which is finite in both directions, if it is possible to connect the sites at the ends of one direction with a complex long-range hopping, we can realize this cylinder geometry with a flux. This might be easier using a synthetic dimension [66]. A second possible way is discussed in Ref. [67]. It proposes to use Laguerre-Gauss beams to create a cylinder optical lattice. Another possibility is to engineer a ring shaped system with the central hole pierced by a tunable magnetic flux, as it can be realized using the scheme proposed in Ref. [68]. For the charge pump measurement, as we have shown for the non-interacting case with rate equations, there is the possibility to couple the system weakly to a low-temperature heat bath to prepare the system in a state close to equilibrium. Bath engineering can be used to reach sufficiently low effective temperatures in the NESS. Then, the flux can be adiabatically ramped up to have a pronounced charge pump.

We have a comment on the bath. To study NESS in a driven system, it is necessary to connect the system to a bath to dissipate the extra energy. Most setups for cold atoms in optical lattices are isolated systems, but they can be in the prethermal regime when the driving frequency is sufficiently large. We may expect that the NESS in our setup may share some similarities for an isolated system in the prethermal regime [69].

IV. CONCLUSION

In conclusion, we have studied the charge density wave and charge pump of fermions with Falicov-Kimball inter-actions in a circularly shaken hexagonal optical lattice. We show that the charge density wave is induced by the staggered potential and is dramatically changed because of resonant tunneling. We also show interaction effects on the topological properties. An increase of the Falicov-Kimball interaction tends to smear out the edge states, and finally makes the system enter the Mott insulator phase.

Furthermore, we study non-equilibrium steady states in a Laughlin charge pump setup which is coupled to either a fermionic reservoir or a heat bath. In the interacting case, we show that the charge pump is not integer for insertion of one flux quantum. Also for the non-interacting case, we find that it is not integer due to dissipation into a bath. We confirm this by detailed calculations via rate equations based on the Floquet-Born-Markov approximation. Moreover, we explored possibilities to lower the effective temperature characterizing the NESS of the driven system by engineering the spectral properties of the bath. Our calculations suggest that in theory one can indeed use the presence of a bath to cool down the system, e.g. after a quench where in the closed system typically there are excitations in the upper band, and also to some extent one can overcome the heating that is inherent in the interacting Floquet system. We propose an experimentally feasible procedure to ramp up the flux for the measurement of the charge pump.

In the future, the approaches developed here can also be applied to the Haldane-Hubbard model, where both spin states are mobile, and which is naturally realized with cold atoms in optical lattices.

V. ACKNOWLEDGMENTS

[1] A. Eckardt, Rev. Mod. Phys. **89**, 011004 (2017).

[2] N. Goldman, J. C. Budich, and P. Zoller, Nat. Phys. **12**, 639 (2016).

[3] M. Aidelsburger, M. Atala, M. Lohse, J. T. Barreiro, B. Paredes, and I. Bloch, Phys. Rev. Lett. **111**, 185301 (2013).

[4] H. Miyake, G. A. Siviloglou, C. J. Kennedy, W. C. Bur-ton, and W. Ketterle, Phys. Rev. Lett. **111**, 185302 (2013).

[5] M. Aidelsburger, M. Lohse, C. Schweizer, M. Atala, J. T. Barreiro, S. Nascimbene, N. R. Cooper, I. Bloch, and N. Goldman, Nat. Phys. **11**, 162 (2015).

[6] G. Jotzu, M. Messer, R. Desbuquois, M. Lebrat, T. Uehlinger, D. Greif, and T. Esslinger, Nature **515**,

237 (2014).

[7] N. Fläschner, B. S. Rem, M. Tarnowski, D. Vogel, D. S. Lühmann, K. Sengstock, and C. Weitenberg, Science **352**, 1091 (2016).

[8] N. Fläschner, D. Vogel, M. Tarnowski, B. S. Rem, D. S. Lühmann, M. Heyl, J. C. Budich, L. Mathey, K. Sengstock, and C. Weitenberg, Nat. Phys. (2017), 10.1038/s41567-017-0013-8.

[9] H.-I. Lu, M. Schemmer, L. M. Aycock, D. Genkina, S. Sugawa, and I. B. Spielman, Phys. Rev. Lett. **116**, 200402 (2016).

[10] M. Lohse, C. Schweizer, O. Zilberberg, M. Aidelsburger, and I. Bloch, Nat. Phys. **12**, 350 (2016).

[11] S. Nakajima, T. Tomita, S. Taie, T. Ichinose, H. Ozawa, L. Wang, M. Troyer, and Y. Takahashi, Nat Phys **12**, 296 (2016).

[12] M. Lohse, C. Schweizer, H. M. Price, O. Zilberberg, and I. Bloch, Nature **553**, 55 (2018).

[13] P. Hauke, M. Lewenstein, and A. Eckardt, Phys. Rev. Lett. **113**, 045303 (2014).

[14] M. Tarnowski, F. N. Ünal, N. Fläschner, B. S. Rem, A. Eckardt, K. Sengstock, and C. Weitenberg, arXiv: 1709.01046 (2017).

[15] C. Wang, P. Zhang, X. Chen, J. Yu, and H. Zhai, Phys. Rev. Lett. **118**, 185701 (2017).

[16] L. D'Alessio and M. Rigol, Phys. Rev. X **4**, 041048 (2014).

[17] A. Lazarides, A. Das, and R. Moessner, Phys. Rev. E **90**, 012110 (2014).

[18] P. Ponte, Z. Papić, F. m. c. Huveneers, and D. A. Abanin, Phys. Rev. Lett. **114**, 140401 (2015).

[19] A. Lazarides, A. Das, and R. Moessner, Phys. Rev. Lett. **115**, 030402 (2015).

[20] A. Lazarides, A. Das, and R. Moessner, Phys. Rev. Lett. **112**, 150401 (2014).

[21] M. Bukov, S. Gopalakrishnan, M. Knap, and E. Demler, Phys. Rev. Lett. **115**, 205301 (2015).

[22] S. A. Weidinger and M. Knap, Sci. Rep. **7**, 45382 (2017).

[23] M. Weinberg, C. Ölschläger, C. Sträter, S. Prelle, A. Eckardt, K. Sengstock, and J. Simonet, Phys. Rev. A **92**, 043621 (2015).

[24] F. Görg, M. Messer, K. Sandholzer, G. Jotzu, R. Desbuquois, and T. Esslinger, Nature **553**, 481 (2018).

[25] M. Reitter, J. Näger, K. Wintersperger, C. Sträter, I. Bloch, A. Eckardt, and U. Schneider, Phys. Rev. Lett. **119**, 200402 (2017).

[26] N. Goldman and J. Dalibard, Phys. Rev. X **4**, 031027 (2014).

[27] M. Bukov, L. D'Alessio, and A. Polkovnikov, Adv. Phys. **64**, 139 (2015).

[28] A. Eckardt and E. Anisimovas, New J. Phys. **17**, 093039 (2015).

[29] W. Zheng, H. Shen, Z. Wang, and H. Zhai, Phys. Rev. B **91**, 161107 (2015).

[30] K. Plekhanov, G. Roux, and K. Le Hur, Phys. Rev. B **95**, 045102 (2017).

[31] E. Anisimovas, G. Žlabys, B. M. Anderson, G. Juzeliūnas, and A. Eckardt, Phys. Rev. B **91**, 245135 (2015).

[32] M. Bukov, M. Kolodrubetz, and A. Polkovnikov, Phys. Rev. Lett. **116**, 125301 (2016).

[33] J. K. Freericks, V. M. Turkowski, and V. Zlatić, Phys. Rev. Lett. **97**, 266408 (2006).

[34] N. Tsuji, T. Oka, and H. Aoki, Phys. Rev. B **78**, 235124

[35] (2008).

[35] A. V. Joura, J. K. Freericks, and T. Pruschke, Phys. Rev. Lett. **101**, 196401 (2008).

[36] J. K. Freericks and A. V. Joura, "Nonequilibrium density of states and distribution functions for strongly correlated materials across the mott transition," in Electron Transport in Nanosystems, edited by J. Bonča and S. Kruchinin (Springer Netherlands, Dordrecht, 2008) pp. 219–236.

[37] H. Aoki, N. Tsuji, M. Eckstein, M. Kollar, T. Oka, and P. Werner, Rev. Mod. Phys. **86**, 779 (2014).

[38] R. B. Laughlin, Phys. Rev. B **23**, 5632 (1981).

[39] R. Sohal and A. Eckardt, Draft (2016).

[40] N. Tsuji, Theoretical Study of Nonequilibrium Correlated Fermions Driven by ac Fields, Ph.D. thesis, Department of Physics, University of Tokyo (2010).

[41] T. Qin and W. Hofstetter, Phys. Rev. B **96**, 075134 (2017).

[42] N. Tsuji, T. Oka, and H. Aoki, Phys. Rev. Lett. **103**, 047403 (2009).

[43] J. Rammer, Quantum Field Theory of Non-equilibrium States (Cambridge University Press, 2007).

[44] H. Breuer and F. Petruccione, The Theory of Open Quantum Systems (Oxford University Press, Oxford & New York, 2002).

[45] S. Kohler, R. Utermann, P. Hänggi, and T. Dittrich, Phys. Rev. E **58**, 7219 (1998).

[46] D. W. Hone, R. Ketzmerick, and W. Kohn, Phys. Rev. E **79**, 051129 (2009).

[47] C. Cohen-Tannoudji, Atoms in electromagnetic fields, Vol. 1 (World scientific, 1994).

[48] D. Vorberg, W. Wustmann, R. Ketzmerick, and A. Eckardt, Phys. Rev. Lett. **111**, 240405 (2013).

[49] D. Vorberg, W. Wustmann, H. Schomerus, R. Ketzmerick, and A. Eckardt, Phys. Rev. E **92**, 062119 (2015).

[50] L. Chen, J. K. Freericks, and B. A. Jones, Phys. Rev. B **68**, 153102 (2003).

[51] O. P. Matveev, A. M. Shvaika, and J. K. Freericks, Phys. Rev. B **77**, 035102 (2008).

[52] H.-S. Nguyen and M.-T. Tran, Phys. Rev. B **88**, 165132 (2013).

[53] T. Qin and W. Hofstetter, Phys. Rev. B **97**, 125115 (2018).

[54] L. Wang, H.-H. Hung, and M. Troyer, Phys. Rev. B **90**, 205111 (2014).

[55] A. G. Grushin, J. Motruk, M. P. Zaletel, and F. Pollmann, Phys. Rev. B **91**, 035136 (2015).

[56] M. P. Zaletel, R. S. K. Mong, and F. Pollmann, J. Stat. Mech. Theory. Exp. **2014**, P10007 (2014).

[57] Q. Niu, D. J. Thouless, and Y.-S. Wu, Phys. Rev. B **31**, 3372 (1985).

[58] X.-L. Qi, Y.-S. Wu, and S.-C. Zhang, Phys. Rev. B **74**, 045125 (2006).

[59] T. Shirai, J. Thingna, T. Mori, S. Denisov, P. Hänggi, and S. Miyashita, New J. Phys. **18**, 053008 (2016).

[60] T. Iadecola, T. Neupert, and C. Chamon, Phys. Rev. B **91**, 235133 (2015).

[61] K. I. Seetharam, C.-E. Bardyn, N. H. Lindner, M. S. Rudner, and G. Refael, Phys. Rev. X **5**, 041050 (2015).

[62] H. Dehghani, T. Oka, and A. Mitra, Phys. Rev. B **91**, 155422 (2015).

[63] A. Klein and M. Fleischhauer, Phys. Rev. A **71**, 033605 (2005).

[64] P. Ostmann and W. T. Strunz, arXiv: 1707.05257

(2017).

[65] M. Messer, R. Desbuquois, T. Uehlinger, G. Jotzu, S. Huber, D. Greif, and T. Esslinger, Phys. Rev. Lett. **115**, 115303 (2015).

[66] O. Boada, A. Celi, J. Rodríguez-Laguna, J. I. Latorre, and M. Lewenstein, New J. Phys. **17**, 045007 (2015).

[67] M. Łącki, H. Pichler, A. Sterdyniak, A. Lyras, V. E. Lembessis, O. Al-Dossary, J. C. Budich, and P. Zoller, Phys. Rev. A **93**, 013604 (2016).

[68] B. Wang, F. N. Ünal, and A. Eckardt, arXiv: 1802.06815 (2018).

[69] D. V. Else, B. Bauer, and C. Nayak, Phys. Rev. X **7**, 011026 (2017).